Journal listed in Halu Oleo University Journal System

International Journal of Acta Material

Int. J. Act. Mat.

homepage: https://ijacmat.uho.ac.id/index.php/journal

Research Article

The Effect of Doping Concentration in the Work Electrodes of Graphene-Mn_xO_y and Test on Glucose by Cyclic Voltametry

L. Agusu[a*], T. Azis[b], Imran[b], Fitrianti[b], A. T. Nurwahida[c]

[a] *Department of Physic, Faculty of Mathematics and Natural Sciences, Halu Oleo University, Kampus Hijau Bumi Tridharma, Anduonohu, Kendari, Sulawesi Tenggara 93232, Indonesia*

[b] *Department of Chemistry, Faculty of Mathematics and Natural Sciences, Halu Oleo University, Kampus Hijau Bumi Tridharma, Anduonohu, Kendari, Sulawesi Tenggara 93232, Indonesia*

[c] *Department of Pharmacy, Bani Saleh University, Jalan Mayor M. Hasibuan No 68. Bekasi Timur 17113, Jawa Barat, Indonesia*

[*] *Corresponding Author: la_agusu@yahoo.com*

Article info

Received: June 2024
Received in revised: July 2024
Accepted: August 2024
Available online: August 2024

Abstract

A study was conducted to investigate the impact of concentration on the graphene-manganese oxide (EPG/Mn_xO_y) working electrode for glucose analysis using the cyclic voltammetry method. To characterize the electrode material, SEM-EDX, FTIR, and XRD analyses were performed. The results revealed that the graphene surface contained aggregates in the form of small particles attached to the graphene. Various absorption bands corresponding to aliphatic -O-H, -C-H, -C=C aromatic, -C=O, -C=C, -C-O, and Mn-O groups were identified in the graphene and graphene/Mn_xO_y materials. Crystal patterns of manganese oxide were also identified at angles 2θ = 30.57° and 44.39°, representing the Mn_3O_4 crystal pattern, at the angle 2θ=34.12° denoting the MnO_2 crystal pattern, and at angles 2θ: 39.85°, 57.85°, and 68.94° representing the MnO crystal patterns. The optimal electrode composition was found to be graphene:Mn_xO_y 0.8:0.5, as indicated by an anodic peak current (Ipa) of 122 µA at a potential of -0.11 V. The most effective supporting electrolyte was determined to be $NaNO_3$, with an anodic peak current (Ipa) of 26.4 µA at a potential of -0.13 V. The detection limit for glucose was 4.45×10^{-3} M. The repeatability test of EPG/Mn_xO_y yielded a result of 1.77%.

 Keywords: EPG/Mn_xO_y, $NaNO_3$, glucose, voltammetry, cyclic voltammetry

INTRODUCTION

Glucose is a vital type of carbohydrate that serves as an energy source for humans, animals, and plants (Fessenden, 1995). When glucose levels in the body surpass a certain threshold, it can lead to a disease known as diabetes mellitus (DM). The pancreas plays a crucial role in regulating glucose levels by producing insulin. Any dysfunction in insulin production can disrupt the pancreas' function. Abnormal glucose levels are characterized by an increase or decrease in the reference range of 60-110 mg/dL (Bantounou et al., 2024).

The biosensor method, introduced by Clark and Lyson in 1962, is commonly used to determine glucose levels. However, this method has limitations due to the susceptibility of the enzymes used to damage, resulting in relatively short-term use. High-performance liquid chromatography (HPLC) and electrochemical methods are alternative approaches for specific glucose determination (Ayati et al., 2023; Wang, Zheng, Huang, Ma, & Zhao, 2024). Ratnayani, Adhi, & Gitadewi, (2008) analyzed glucose and fructose levels using the HPLC method, which

has the drawback of being unable to simultaneously analyze multiple sample types and being costly. Kamal & Klein, (2011) determined the sugar content in honey using the LC-MS method, which provides more specificity by enabling the determination of individual sugars such as fructose, glucose, sucrose, and even maltose when present. However, this method comes with a relatively high analysis cost.

Given these challenges, there is a need for a simpler and cost-effective alternative method that retains sensitivity to glucose. The electrochemical method, which analyzes samples based on reduction and oxidation reactions occurring on the electrode surface, proves to be a suitable choice. Electrochemical cells establish relationships between concentration and potential (potentiometry), concentration and electrical conductivity (conductometry), concentration and amount of electrical charge (coulometry), and concentration with potential and electric current (polarography and voltammetry) (Esfandiari & Aliofkhazraei, 2024; Han & Priefer, 2023).

Among the various electrochemical methods, cyclic voltammetry focuses on the correlation between electrical quantities and chemical reactions. This method offers advantages such as low detection limits, high selectivity, easy sample preparation, and cost-effectiveness compared to other methods. Cyclic voltammetry employs three types of electrodes, with the working electrode being the most influential in performance. The working electrode serves as the site for redox reactions. Carbon, platinum, and gold are commonly used as working electrodes, with carbon electrodes, particularly those based on graphene, gaining prominence in electroanalysis due to their wide potential range, low background current, affordability, inertness, and compatibility with various sensors (Nur Ashakirin Binti Mohd Nashruddin, Hani Mohamed Salleh, & Ayunni Mohd Raub, 2024; Wong, Yokota, & Kim, 2022) .

Graphene is a monolayer of graphite, characterized by sp^2 hybridization of carbon atoms arranged in a hexagonal structure within a honeycomb crystal lattice (Othman et al., 2024). This two-dimensional carbon material possesses a specific surface area (Stoller, Park, Zhu, An, & Ruoff, 2008) and a honeycomb structure that exhibits potential for higher lithium storage capacity, enhanced electron mobility, and excellent electrical conductivity. The remarkable electrical conductivity of graphene facilitates facile electron exchange between analyte molecules, making it an excellent choice as a base material for working electrodes in voltammetric cells. Moreover, the performance of graphene working electrodes can be enhanced through the incorporation of modifiers, with titanium dioxide (TiO_2) being the most commonly employed modifier (Alanezi et al., 2024; Sharma et al., 2024). Another potential modifier that can be utilized is manganese oxide (Mn_xO_y).

Manganese oxide is a nanomaterial of significant interest due to its diverse applications. The application of manganese oxide is closely linked to its structural characteristics. For example, manganese oxide with a hollow structure, such as cryptomelane, can serve as a catalyst, ion exchanger, and absorbent (Li et al., 2022). On the other hand, manganese oxide with a larger cavity structure, specifically todorrokite, exhibits great potential as a catalyst and absorbent. Furthermore, manganese oxide with the smallest cavity structure, namely pyrolusite, finds widespread use in the glass and battery industries (Chung, Heaney, Post, Stubbs, & Eng, 2023). In addition to its hollow structure, manganese oxide also possesses a layered structure known as birnessite, which can be utilized as an ion exchange material and as a cathode material for lithium batteries (Liang et al., 2024). Building upon the aforementioned context, the present study aims to expand upon previous research by investigating the utilization of graphene working electrodes with Mn_xO_y modifiers for glucose analysis.

MATERIALS AND METHODS

Materials and Instrument

The materials used in this research are graphite, glucose ($C_6H_{12}O_6$), liquid paraffin, potassium permanganate ($KMnO_4$), sulfuric acid (H_2SO_4) 98%, hydrogen peroxide (H_2O_2), sodium nitrate (NaNO), hydrochloric acid (HCl) 37%, manganese rock, sodium hydroxide (NaOH), potassium ferricyanide ($K_3[Fe(CN)_6]$), and distilled water. The tools used in this research are potentiostats DY2100B, platinum electrode, Ag/AgCl (saturated KCl) reference electrode, body electrode, copper wire, beaker (Iwaky Pyrex) 50 mL, 100 mL and 250 mL, measuring cup (Iwaky Pyrex) 25 mL, measuring flask (Iwaky Pyrex) 100 mL, pipette measuring (Iwaky Pyrex)

5 mL and 10 mL, micro pipette, centrifuge, hydrothermal autoclave, oven (Gallenkamp England), porcelain cup, dropper, filler, mortal, 250 mesh sieve, hot plate stirrer, ice bath, ultrasonication, stir bar, tweezers, spray bottle, stand and clamp, pH meter, scale (Exploler Ohaus: max. 210 g and min. 0.001 mg), spatula, tongs, X-Ray Diffraction (XRD) (Shimadzu 6000), Fourier Transform InfraRed (FTIR) (Shimadzu 8400) and Scanning Electron Microscopy (SEM) (brand HITACHI SU3500).

Synthesis of graphite oxide

Graphite oxide was synthesized using a modified Hummer method. The synthesis process involves utilizing graphite powder, $KMnO_4$, and H_2SO_4 as primary materials. To start, 2 g of graphite powder and 4 g of $NaNO_3$ were stirred with 98 mL of H_2SO_4 (98%) for 4 hours at a high speed in an ice bath. After 1 hour of stirring, 8 g of $KMnO_4$ and 4 g of $NaNO_3$ were gradually added. The stirring process was continued at a temperature of 25°C for 24 hours. Subsequently, 200 mL of distilled water was gradually added to the solution and stirred for approximately 1 hour until homogeneity was achieved. Following this, 15 mL of hydrogen peroxide was gradually added while stirring. The solution was then separated into solid and liquid phases using a centrifuge operating at a speed of 3000 rpm for 1 hour. The solid phase obtained from the separation was washed several times using 10 mL of 37% HCl and distilled water until the pH of the solution reached neutrality. If there are any remaining sulfate ions (SO^{-4}), the drying process of the graphite oxide is carried out in an oven at a temperature of 110°C for 12 hours (Agusu & Yuliana, 2017)

Synthesis of graphene oxide

In a 100 mL volume of distilled water, dissolve 0.4 g of graphite oxide until a homogeneous solution is obtained. Once homogeneous, sonicate the solution for 3 hours at a temperature of 100 ^oC. This process will cause the exfoliation of graphite oxide into graphene oxide.

Manganese oxide leaching

The leaching of manganese oxide begins by dissolving 20 g of natural manganese powder in 50 mL of 37% HCl. The solution stired for approximately 3 hours at a temperature of 70 ^oC, or until a homogeneous solution is achieved. Next, perform filtering to eliminate any impurities.

Reduction and doping of graphene oxide with manganese oxide

To initiate this process, dissolve 0.8 g of graphene oxide in each previously prepared filtrate of manganese oxide. The ratios for the mixtures should be 8:2, 8:4, and 8:6, respectively. Each mixture stirred for 30 minutes. Next, subject the homogenized graphene oxide and manganese oxide to ultrasonication at a frequency of 53 kHz for a duration of 2 hours. Subsequently, employ a hydrothermal autoclave at a temperature of 180ºC for 24 hours. The graphene, now doped with manganese oxide, is then dried at a temperature of 110ºC for 24 hours.

Preparation of working electrodes (graphene-manganese oxide)

The preparation of the working electrodes involves grinding graphene/manganese oxide to achieve a smooth consistency. This mixture is then transferred to a watch glass containing paraffin, which is heated to a temperature of 80^oC. The mixture is thoroughly stirred and subsequently inserted into the electrode body to solidify. Once solidified, the surface of the electrode is carefully polished to achieve a smooth, even, and glossy finish. This process yields three working electrodes, each synthesized with varying concentrations of manganese oxide previously prepared.

Characterization of Graphene-Mn Oxide

The characterization of the Graphene-Mn Oxide composite involved the analysis of the most widely recognized manganese oxide concentration, based on the previously prepared voltammogram of each electrode.

Characterization of manganese oxide-doped graphene paste electrodes

The electrodes were subjected to testing using the Cyclic Voltammetry (CV) method to determine the redox peak and current strength. The electrode testing was conducted using a three-electrode system, consisting of a *graphene*-Mn_xO_y graphene paste electrode as the working electrode, Ag/AgCl as the reference electrode, and platinum wire as the auxiliary electrode. The three electrodes were inserted into the electrochemistry cell containing a 0.01 M $K_3[Fe(CN)_6]$ solution. The measurements were

then taken over a potential range from -0.8V to 0.8V, with a scan rate of 0.05 V/s (Irdawati, Manurung, & Septiawan, 2015a) At this stage, three tests were conducted on each working electrode with different compositions, as prepared beforehand.

Graphene/Mn_xO_y Electrode Performance Testing

Testing the Impact of Electrolytes on the Performance of Graphene/Mn_x Electrodes in Glucose Analysis

EPG/Mn_xO_y electrodes were inserted into a voltammetry cell containing a 10 mL solution of 0.1 M glucose and a 10 mL solution of a supporting electrolyte with various electrolytes: 0.1 M H_2SO_4, 0.1 M NaOH, and 0.1 M $NaNO_3$. Current measurements were then conducted at a potential range of -0.8 V to 0.8 V with a scan rate of 0.5 V/s. The obtained voltammograms were compared to determine the most effective supported electrolyte.

Graphene/MnxOy Electrode Performance Test for Glucose Detection

The EPG/Mn_xO_y composition that yielded the best results was tested in a voltammetry cell containing a 0.01 M glucose solution. The resulting voltammogram was then compared to the voltammogram obtained when EPG/Mn_xO_y was tested in a 0.1 M $NaNO_3$ electrolyte solution.

Determination of Linearity Area and Limit of Detection (LOD)

Peak current of glucose test solutions 10^{-5}, 10^{-4}, 10^{-3}, 10^{-2} using the CV method. The current response from the resulting voltammogram is plotted against the concentration and the linear region of the calibration curve is determined. The measurement detection limit refers to the minimum concentration at which an analyte signal can still be measured by the instrument. This detection limit (DL) is calculated using Equation 1,

$$DL = (3 \times S_a) / b \quad (1)$$

Where S_a denotes the standard deviation and b represents the slope of the curve.

Measurement Repeatability Analysis

The assessment of measurement repeatability was conducted by utilizing the EPG/Mn_xO_y electrode. A total of 11 measurements were taken on a 0.01 M glucose test solution in a $NaNO_3$ supporting electrolyte solution. The repeatability was determined based on the peak current values obtained from each measurement, as well as the *Relative Standard Deviation* (RSD) (Equation 2) and the *Relative Standard Deviation Horwitz* ($PRSD_R$) (Equation 3) values for EPG/MnO.

$$\%RSD = \frac{SD}{X} x\ 100\% \quad (2)$$

$$\%\ PRSD_R = 2^{1-(0.5 \log 0.01)} \quad (3)$$

Where, DS= Standard deviation, X= Average value of current, C = Concentration of glucose test solution. Repeatability of measurements is declared good if the Horwitz Ratio (HorRat) value less than 2. HorRat value is the comparison of %RSDR and %PRSDR (Albert & Horwitz, 1997).

Evaluating Graphene/Mn_x Electrode Performance in Glucose Determination

In this study, a 0.1 M glucose solution in $NaNO_3$ electrolyte solution (10 mL) was monitored over a period of 15 days, with measurements taken daily. The voltammogram analysis of the measurement results from the first to the fifteenth day provides valuable insights into the age and performance of the electrode.

RESULTS AND DISCUSSION

Graphene Synthesis

Graphene synthesis is carried out using several methods and the most widely used is the modified Hummer method (Hummers & Offeman, 1958) where this method uses various chemical reactions to oxidize graphite to graphite oxide. Graphene has various unique chemical and physical properties and various potentials that can be used in technological applications, so methods in the process of producing graphene are important to research.

Graphene synthesis begins with the synthesis of graphite oxide using graphite powder as a precursor for the formation of graphene. $KMnO_4$ functions as an oxidizing agent, $NaNO_3$ as a catalyst and H_2SO_4 as a solvent. The reactions that occur in the graphite oxidation process by $KMnO_4$ can be seen in Equations (4) and (5) (R. Dreyer, Park, W. Bielawski, & S. Ruoff, 2010). This oxidation process only takes place in an acidic

environment, so H_2SO_4 also acts as a maker of acidic conditions in the solution.

$$KMnO_4+3H_2SO_4 \longrightarrow K^+ + MnO_3^+ + H_3O^+ + 3HSO_4^- \quad (4)$$

$$MnO_3^+ + MnO_4^- \longrightarrow Mn_2O_7 \quad (5)$$

The oxidation process involved in the synthesis of graphene entails the production of graphite oxide. Under acidic conditions, an oxidation reaction occurs, leading to a noticeable color change in the mixture from dark green to dark brown. This alteration signifies the initiation of the graphite oxidation process resulting from the reaction between graphite, H_2SO_4, and $KMnO_4$. Consequently, various functional groups, such as phenol groups, epoxy groups, ketone groups, carboxyl groups, and carbonyl groups, are formed and subsequently bound to graphite (Shao et al., 2012). These functional groups render graphite oxide highly hydrophilic and prone to easy exfoliation, forming graphene oxide.

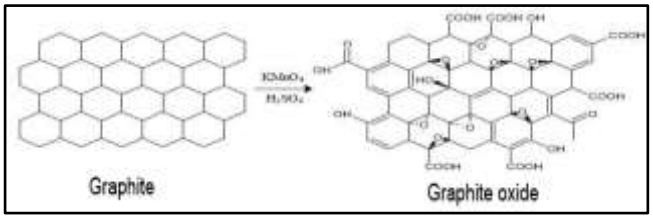

Figure 1. Graphite Oxidation Reaction to Graphite Oxide

The next stage involves the synthesis of graphene oxide from graphite oxide. Graphite oxide undergoes exfoliation in water using the sonication method at a frequency of 53 kHz. This exfoliation process is driven by ultrasonic waves with a frequency range exceeding 20 kHz and occurs mechanically. The exfoliation of graphite oxide is induced by the interaction with ultrasonic waves and the cavitation process, which refers to the change in the vapor phase of a liquid due to pressure reduction below the saturated vapor pressure. This cavitation process occurs within the medium, specifically water, leading to a displacement in the graphite oxide layers. The pressure differentials during the ultrasonication process result in the cavitation process and subsequent transformation of graphite oxide into graphene oxide (Ilhami & Susanti, 2014).

Manganese Leaching

This study utilizes naturally occurring manganese from manganese rocks sourced from the Buton district in Southeast Sulawesi. Natural manganese has the ability to form various manganese oxide compounds, such as Manganese (II) Oxide (MnO), Manganese (IV) Oxide (MnO_2), Manganese (III) Oxide (Mn_2O_3), and Manganese (II,III) Oxide (Mn_3O_4).

The synthesis process of manganese oxide begins by dissolving the natural manganese in 37% HCl. Hydrochloric acid (HCl) acts as a solvent that affects the purity level of the manganese obtained. The purity of natural manganese increases with a higher concentration of HCl. As a strong acid, HCl can dissolve manganese oxide from its ore into Mn^{2+}, Mn3+, Mn^{4+}, Mn^{6+}, and Mn^{7+} ions. Solutions containing these ions are crucial as the foundation for the production of manganese oxide nanoparticles. The solubility of HCl influences the surface area of the manganese oxide particles. Smaller particles have a greater collision rate with the solvent, resulting in their dissolution (Mira, Mahmudin, & Iqbal, 2018). The dissolution of natural manganese is indicated by the formation of a yellowish-brown solution (Figure 2).

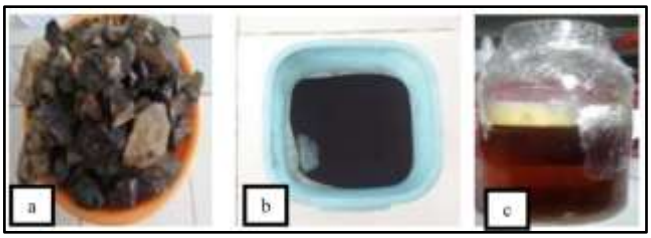

Figure 2. (a) Natural Manganese (b) Natural Manganese Powder (c) Leaching Solution

The leaching process, involving the washing or dissolution of manganese from its ore using hydrochloric acid, was proposed and patented by Abdrashitov (2001). In this process, Mn ore can dissolve in a 5% water-20% HCl solution, leading to the formation of $MnCl_2$ (Zhang & Cheng, 2007), as shown in the following reaction (Equation 6 and 7).

$$MnO + 2HCl \rightarrow MnCl_2 + H_2O \quad (6)$$

$$Mn_3O_4 + 4HCl \rightarrow MnO_2 + 2MnCl_2 + 2H_2O \quad (7)$$

Graphene Oxide Doped with Manganese Oxide

The synthesized graphene oxide was doped with a leached manganese solution to combine two different materials and enhance their properties (Arifiyana & Murwani, 2013). The doping process involved three variations of manganese (0.1 grams, 0.3 grams, and 0.5 grams) to determine the optimal composition of manganese oxide dopant on the performance of the graphene/MnxOy electrode.

The synthesis of the graphene/Mn_xO_y composite consisted of two stages: sonication and hydrothermal processes. During sonication, manganese was dispersed into the graphene nanocomposite using ultrasonic waves for 30 minutes at a frequency of 53 Hz to produce manganese oxide doped graphene material. The sonicator tool provided a chemical effect on ultrasonication, facilitating molecular interaction and chemical changes. The temperature increased from 30 °C to 42 °C due to the influence of continuous ultrasonic waves (Figure 3a).

Figure 3. (a) Sonication process (b) Hydrothermal

The Mn-graphene interaction was then followed by the hydrothermal process to form a graphene-Mn composite. The hydrothermal process was conducted for 24 hours at 180 °C (Figure 3b) to achieve good crystal formation under low temperature and pressure. Manganese oxide (MnxOy) served dual functions as a reducing agent and dopant in the graphene oxide nanocomposites. The interaction between Mn ions and graphene involved the formation of phi (π) bonds, facilitating electron exchange.

Based on research by Alimin, Narsito, Kartini, & Santosa, (2015), it can be inferred that graphene acts as a reducing agent, enabling the growth of metal ions into nanoparticles. This occurs when Mn interacts with the benzene ring in graphene, where the phi (π) electrons in the benzene ring act as acceptors and are donated to the Mn ions, reducing the number of Mn ions sequentially.Based on the reaction mechanism, it is possible to understand the process of manganese oxide formation in the synthesis of graphene/Mn_xO_y nanocomposites. This occurs through reduction and oxidation reactions. The formation of manganese oxide takes place when there is interaction during sonication, leading to the reduction of manganese ions in the graphene nanocomposite. However, this reduction is not complete, resulting in manganese ions that are not fully reduced into graphene. These ions will then undergo another reaction during the hydrothermal process, forming manganese oxide through binding with oxygen.

Desain Graphene/Mn_xO_y Working Electrodes

The production of graphene/Mn_xO_y working electrodes involves the mixing of graphene/Mn_xO_y with liquid paraffin at a ratio of 5:1. This mixture serves as the material for the electrodes (Figure 4). The electrode material is then placed inside the electrode body, which consists of an 8 cm copper (Cu) wire and a 3 cm electrode body with a diameter of 3 mm.

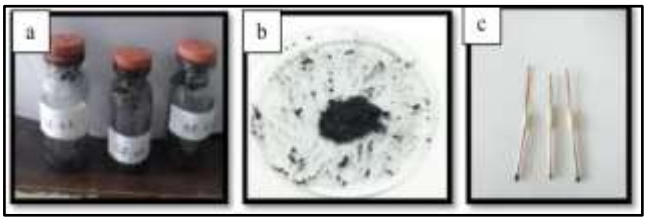

Figure 4. (a) Graphene/Mn material before paraffin mixing (b) graphene/Mn_xO_y paste (c) graphene/Mn_xO_y electrode

Before use, the copper (Cu) wire must be sanded to ensure proper current conduction during the measurement process. Any remaining sandpaper residue on the copper surface should be cleaned using a tissue. Next, the copper wire is inserted into the electrode body, leaving a small empty space at the end for the electrode material. The electrode material is carefully inserted into the electrode body and pressed firmly until it solidifies. The surface of the electrode is then smoothed, ensuring a flat and shiny finish (Figure 5).

Characterization of EPG/MnxOy material

Crystal structure analysis using XRD

Analysis using XRD was carried out to determine the crystal structure of graphite oxide

and graphene that had been synthesized at an angle of 2θ = 20-80^{o} and λ Cu-Kα = 1.54060 Å (Figure 6).

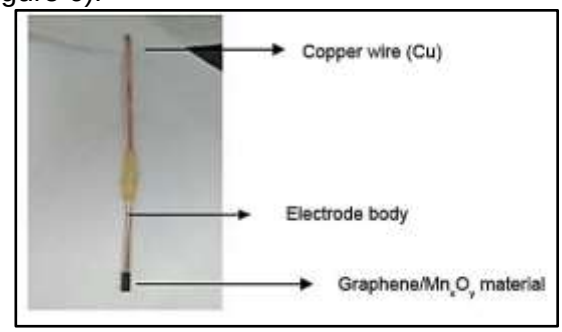

Figure 5. Working electrode components

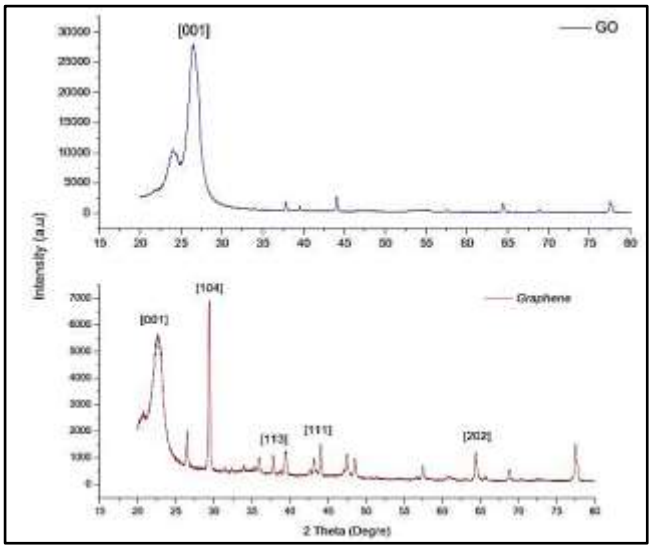

Figure 6. XRD patterns of synthesized graphite oxide and grapheme

The results of XRD analysis revealed an intensity peak of graphite oxide at an angle of 2θ = 26.5149°, with a spacing of 3.359 Å. In graphene, a new peak was observed at 23.04°, with a spacing of 3.857 Å. This finding aligns with the research conducted by Suwadana and Diah (2015), which stated that the highest intensity in graphite oxide is at 2θ = 26.49°, with a spacing of 3.365 Å, while the highest intensity in graphene is at 2θ = 24.86°, with a spacing of 3.578 Å. The change in distance and the leftward shift of the angle occur when graphite oxide transforms into graphene, resulting from the loss of phenol groups, ketone groups, epoxy groups, carboxyl groups, and carbonyl groups (Taufantri, Irdhawati, & Asih, 2016). The larger d-spacing value indicates the reduction of graphite to graphene.

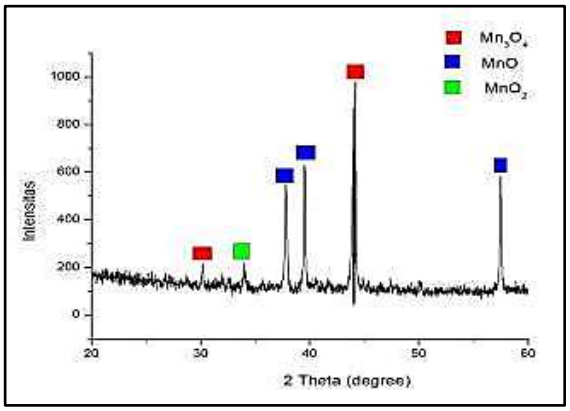

Figure 7. XRD of graphene/Mn$_x$O$_y$

Figure 7 presents the XRD characterization results of graphene/Mn$_x$O$_y$. The pattern indicates the presence of MnO crystal patterns at angles 2θ of 39.85°, 57.85°, and 68.94°, with corresponding d-spacing values of 2.2605 Å, 1.5927 Å, and 1.3610 Å, respectively. Additionally, a peak at an angle of 2θ = 34.12° and d-spacing of 2.6257 Å corresponds to MnO2 crystal. Furthermore, angles 2θ of 30.57° and 44.39°, with d-spacing values of 2.9216 Å and 2.0390 Å, respectively, represent Mn_3O_4 crystal patterns (JCPDS-41-1487).

Figure 7 exhibits XRD diffractograms, revealing characteristic peaks of graphene oxide at 2θ values of 21.03°, 21.57°, and 26.67°. However, these peaks are not distinctly visible due to the overlapping and coverage by the metal oxide resulting from the reaction with carbon. Previous research conducted by (Adhytiawan & Susanti, 2015) indicates that the highest intensity of graphene oxide occurs at the miller index (001) and the corresponding 2θ peak is between 20-25°, which aligns with the Joint Committee Powder Diffraction Standards (JCPDS-41-1487).

Functional Group Analysis Utilizing FTIR

FTIR analysis was conducted to determine the functional groups present in the synthesized graphene/Mn. The wavelength range examined was 300-4500 cm^{-1}. The findings of the FTIR analysis are displayed in Figure 8. Based on the spectrum illustrated in Figure 8, the graphene oxide spectrum exhibits vibrations of the O–H group within the absorption region at 3417.86 cm^{-1}. In contrast, the vibration of the O-H group in the graphene/Mn composite spectrum occurs at a wave number of 3414.00 cm^{-1}.

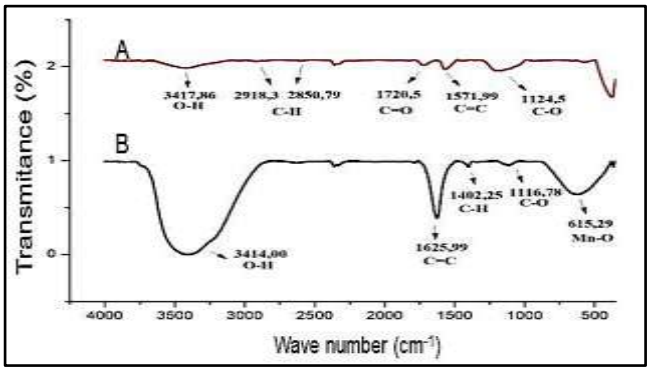

Figure 8. FTIR spectrum of synthesized graphene/Mn (a). Graphene oxide (b). graphene/Mn

The spectrum demonstrates that the O-H group in the graphene/Mn composite exhibits a more pronounced vibration compared to graphene oxide. This can be attributed to an increase in O-H bonds, believed to result from the inclusion of manganese leaching products containing H_2O, as indicated by reaction equations (7) and (8). Aliphatic C–H groups were identified in graphene oxide within wave numbers 2850.79-2918.30 cm^{-1}, whereas in graphene/Mn composites, these groups were observed at a wave number of 1402.25 cm^{-1}.

Furthermore, a C=O group originating from the COOH functional group was detected at a wave number of 1720.50 cm^{-1} in graphene oxide, but absent in graphene/Mn composites. This reduction in graphene is attributed to the presence of Mn ions, leading to a decrease in O atoms within its structure. The vibration of the aromatic C=C group at a wave number of 1571.99 cm^{-1} in graphene transforms into aliphatic C=C (1625.99 cm^{-1}) in graphene/Mn composites. This indicates that the entry of Mn ions has caused damage to the bonds in graphene during the doping process. Additionally, C–O vibrations were observed at wave numbers 1124.50 cm^{-1} in graphene oxide and 1116.78 cm^{-1} in graphene/Mn. The region at wave number 615.29 cm^{-1} was identified as the Mn–O absorption band, consistent with the typical absorption band of manganese oxide within the 700-400 cm^{-1} absorption range, as noted by Prieto (2003). The results obtained from the FTIR analysis confirm the successful doping of manganese oxide into the graphene material.

Surface Morphology Analysis Utilizing Scanning Electron Microscopy

An analysis was performed using scanning electron microscopy (SEM) to evaluate the surface morphology of the graphene/Manganese Oxide working electrode material. The objective was to identify the presence of pore formation and distribution in the sample, with SEM images magnified between 1,000 and 10,000 times (Figure 9).

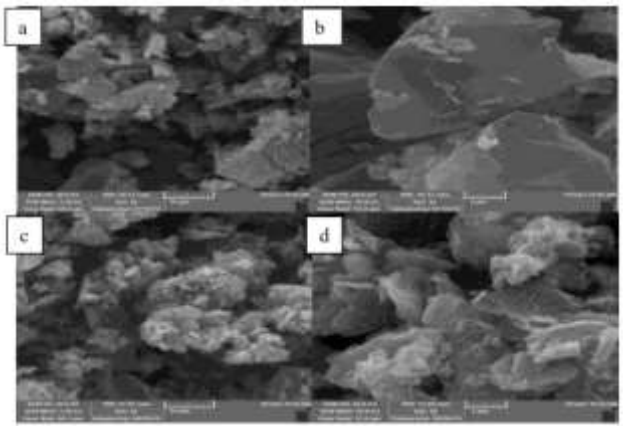

Figure 9. (a) and (b) graphene oxide magnification 2500x and 10000x (c) and (d) graphene/Mn magnification 2500x and 10000x

Based on the results of SEM analysis shown in Figure 9, it is evident that there are variations in the surface morphology between graphene oxide and graphene/Mn composites. In Figure 9 (a) and (b), the surface of graphene oxide appears as thin and smooth sheets, contrasting with Figure 9 (c) and (d) where the surface is rough due to the presence of granular particles adhering to it. These observations suggest that the sheet-like particles correspond to graphene sheets, while the granular particles are manganese oxide particles. This finding aligns with the study conducted by (Song & Ma, 2018), wherein they synthesized graphene/Mn3O4 composites and observed a morphological form characterized by Mn_3O_4 grains attaching to the graphene sheet. Consequently, it can be inferred that manganese oxide has been successfully doped onto graphene in this study.

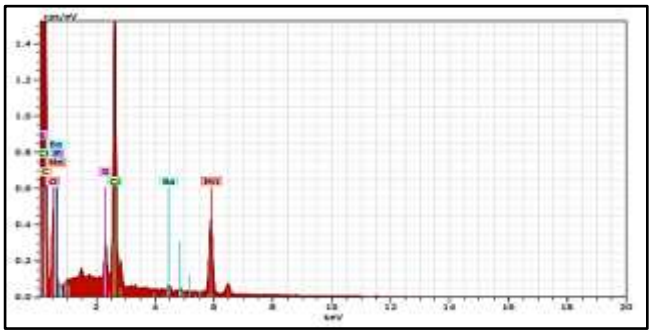

Figure 10. EDX analysis of graphene/Mn_xO_y

Table 1. Composite Components

Elements	Composition (%)
C	76.42
O	16.53
Mn	1.95
Cl	2.98
F	1.7
S	0.36
Ba	0.06

Based on the results of the EDX analysis, the synthesized composite was found to contain various elements, including carbon (C), oxygen (O), and manganese (Mn). Graphene, known for its composition of C and O atoms, accounted for 76.42% and 16.53% of the composite, respectively. The presence of 1.95% Mn atoms suggests the incorporation of manganese into the composite. Additionally, the 2.98% Cl atoms are believed to originate from the solvent used during synthesis. Small percentages of other elements, such as fluorine (F), sulfur (S), and barium (Ba), are also present, likely derived from the natural manganese rock employed.

Characterization of graphene/MnxOy electrode with composition variation in K3[Fe(CN)6] solution

The Manganese Oxide doped graphene electrode with several composition variations was then tested for its performance in K3[Fe(CN)6] solution to determine the best composition and scan rate of the electrode to be used in detecting glucose. Electrode characterization was carried out using 0.01 M $K_3[Fe(CN)_6]$ in 0.1 M $NaNO_3$ supporting electrolyte solution. The supporting electrolyte solution should not produce background current that can affect the measurement of the analyte shown in the voltammogram. Electrodes that are suitable for further testing are electrodes with good oxidation and reduction peak measurements of $K_3[Fe(CN)_6]$. The redox reaction that occurs in the voltammetry cell is shown in Equation 8.

$$Fe(CN)_6^{3-}(aq) + e^- \rightleftharpoons Fe(CN)_6^{4-}(aq) \quad (8)$$

Comparison of anodic and cathodic peak currents shows that the reaction occurring in the $Fe(CN)_6^{3-}/Fe(CN)_6^{4-}$ system is reversible. Tests of graphene/Mn_xO_y electrodes with compositions of 0.8:0.1, 0.8:0.3, and 0.8:0.5 were carried out in $K_3[Fe(CN)_6]$ solution at a scan rate of 0.05 V/s.

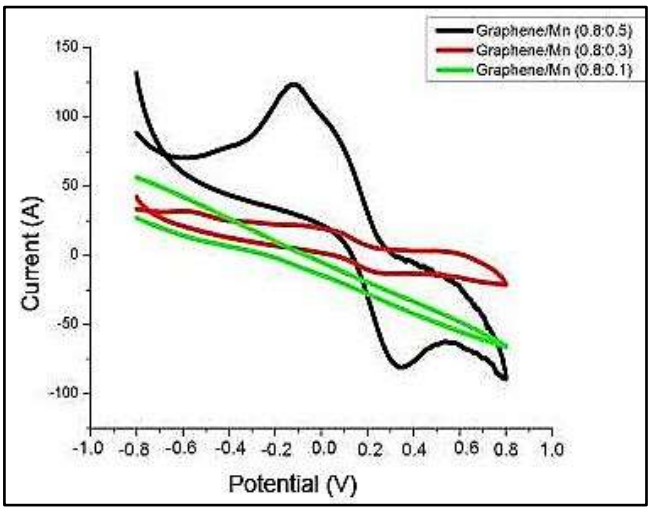

Figure 11. Voltammogram of graphene/MnxOy electrode with composition variation

The voltammogram depicted in Figure 11 demonstrates that the doping composition has an impact on the electrode's performance. In the graphene:Mn_xO_y composition ratio of 0.8:0.5, the voltammogram exhibits a distinctly sharp redox peak without significant widening, distinguishing it from other graphene/Mn_xO_y compositions. This suggests that the redox reaction during the measurement is proceeding effectively. The graphene/Mn_xO_y composition ratio of 0.8:0.5 yields the highest Ipa value of 122 µA at Epa -0.6 V. By analyzing the shape of the voltammogram and the measured oxidation and reduction peak values, it becomes evident that the doping composition significantly impacts the performance of the graphene/Mn_xO_y electrode. The best performance is achieved with a specific composition of graphene and doping, namely 0.8:0.5. In contrast, lower doping compositions result in inferior current production, indicating an inadequate electron transfer process due to insufficient doping. Therefore, the optimal composition for the graphene/Mn_xO_y electrode is

0.8:0.5 grams, as it enhances electrode sensitivity compared to other compositions. Subsequently, this best composition is further optimized in the glucose test solution.

Determining the optimal scan rate

The voltammeter cyclic characteristics are influenced by various factors, including the electron transfer rate, reactivity of electroactive species, and scan rate. Species that are initially oxidized during the forward potential sweep will then be reduced during the reverse potential sweep. In addition to assessing the suitability of the electrode, the voltammogram in the $K_3[Fe(CN)_6]$ solution can also indicate the ability of the modified electrode to amplify the analyte current. The results of the voltammogram, showcasing peaks corresponding to oxidation, reduction, or both, are presented in Figure 12 for the graphene/Mn_xO_y electrode with the optimal composition at various scan rates in the $K_3[Fe(CN)_6]$ solution.

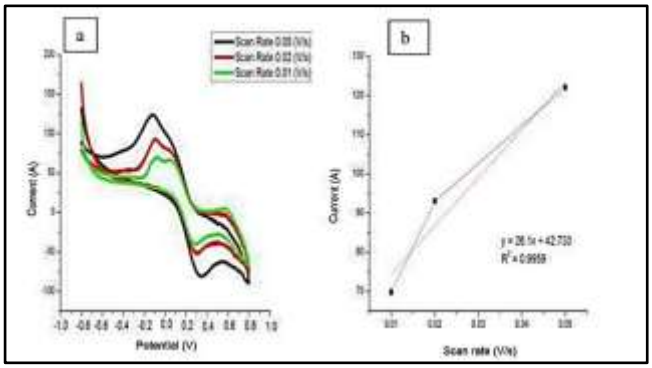

Figure 12. (a) Voltammogram of scan rate variation (b) plot between scan rate and current of $K_3[Fe(CN)_6]$ measurement results.

Based on the results of scan rate variation measurements, it is evident that the optimal scan rate is achieved at a rate of 0.05 V/s. This is supported by the higher I_{pa} value obtained at this scan rate, which registers at 122µA at Epa -0.11 V. Figure 12b illustrates the relationship between scan rate and I_{pa}, with the aim of determining the resulting R^2 value. A R^2 value ranging from 0.9 to 1.0 indicates that the current generated is influenced by the diffusion current. In this particular measurement, the obtained R^2 value is 0.9959, confirming the influence of diffusion current on the current generated from the scan rate measurement.

These findings reveal that the peak current produced increases with higher scan rates. This is attributed to the formation of a thinner diffusion layer at higher scan rates, enabling efficient and rapid electron transfer around the surface of the working electrode. Conversely, lower scan rates result in a thickened diffusion layer on the working electrode surface, hindering electron transfer (Irdawati, Manurung, & Septiawan, 2015b). Consequently, a scan rate of 0.05 V/s is determined to be the most suitable within the range of measurements conducted, and will be utilized in subsequent measurement processes.

Analysis of the impact of supporting electrolytes on the performance of graphene/Mn_xO_y electrodes in glucose analysis

The objective of this study is to investigate the influence of different types of supporting electrolytes on the analysis of 1 M glucose. The supporting electrolyte plays a critical role in maintaining ion strength in solution and supporting the migration current. By comparing the results from each measurement, we aim to identify the optimal conditions for the supporting electrolyte, as illustrated in Figure 13. Based on the measurement results, it is evident that there is a disparity in current between the electrolyte and the glucose test solution. Figure 13 illustrates that the I_{pa} generated during the measurement of glucose in a 0.1 M $NaNO_3$ solution exhibits a relatively higher I_{pa} value of 26.4 µA at Epa -0.13 V.

The determination of the linearity region and limit of detection (LOD) is crucial in assessing the performance of an analytical method. Linearity refers to the capacity of an analysis method to produce a response that is directly proportional to the analyte's concentration. To establish the linear concentration range of glucose measurement, a series of standard glucose solutions with concentrations of 10-5, 10-4, 10-3, 10-2, and 10-1 M in a 0.1 M NaNO3 solution are prepared. By plotting I_{pa} against the concentration of the standard solution, the equation of the linear line can be determined. The measurement results indicate that as the concentration of the test solution increases, the corresponding I_{pa} value also increases.

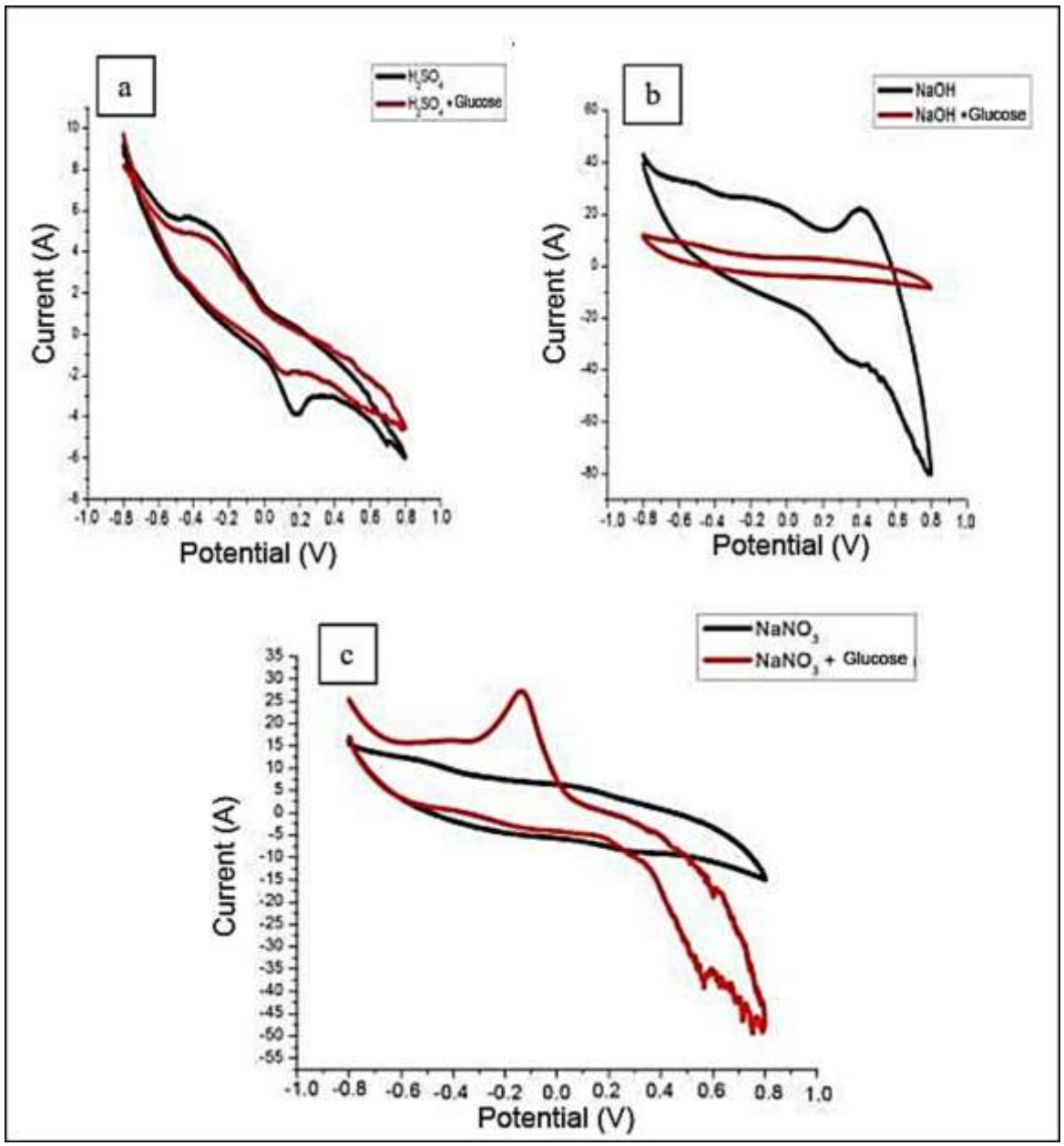

Figure 13. (a) Comparison of H_2SO_4 electrolytes, (b) Comparison of NaOH electrolytes, (c) Comparison of $NaNO_3$ electrolytes

This phenomenon occurs due to the accumulation of ions on the electrode surface, resulting in a higher current. Figure 14 presents the outcomes of the linearity region determination and LOD. The linear concentration of the standard glucose solution was measured in $NaNO_3$ at concentrations ranging from 10^{-5} to 10-1 M. The intercept was determined to be 16.128, with a slope of 1186.2x. Consequently, a linear equation of y=1186.2x + 16.128 was derived. The purpose of establishing this linear curve was to identify the optimal working range for glucose measurement. This concentration range exhibits a linear correlation between glucose concentration and the resulting current in the $NaNO_3$ electrolyte, with an R^2 value of 0.9512. Value of R^2 correlation value within the range of 0.80 - 1.0 indicates a very strong linear relationship.

The detection limit refers to the minimum analyte concentration that can be detected by the analysis procedure. Determining the detection limit for glucose measurement provides insight into the smallest detectable amount of analyte in a sample that still yields a significant

response. Calculation of the detection limit helps identify this threshold. The graphene/Mn_xO_y electrode, when used in conjunction with NaNO3 electrolyte, was found to have a glucose detection limit of 4.45×10^{-3} M based on the measurement results from the glucose concentration series. Consequently, the electrode is capable of detecting glucose concentrations as low as 4.45×10^{-3} M.

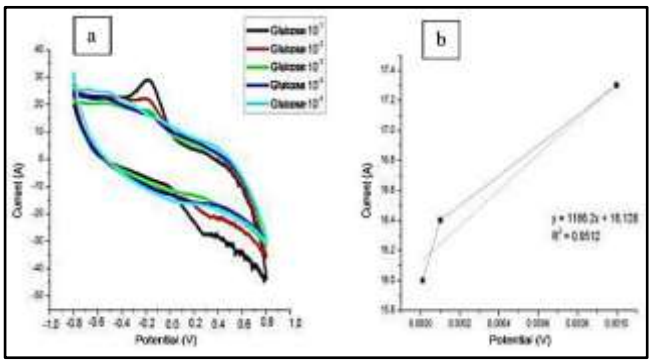

Figure 14. (a) Voltammogram of glucose at a concentration of 10^{-5}- 10^{-1}M in $NaNO_3$ electrolyte (b) Plot between glucose concentration and I_{pa} and linearity region of 10^{-5} - 10^{-3} M in $NaNO_3$ electrolyte.

Determination of measurement repeatability

The measurement variability is one of the precision tests that demonstrates the degree of agreement between individual test results measured through the dispersion of individual results from the mean when the procedure is repeatedly established (Irdawati et al., 2015) The measurement variability of the graphene/Mn_xO_y electrode was performed 11 times on the glucose solution. Subsequently, voltammograms (Figure 15a and 15b) were created between repetitions with the peak current generated in each measurement.

The repeatability of measurements of graphene/Mn_xO_y electrodes can be assessed by calculating the Horwitz Ratio (HorRat) value. The HorRat value is the ratio of %RSDR to %PRSDR of the peak current obtained from the measurement results of a 10-2 M glucose test solution. A HorRat value below 2 and a smaller %RSDR value compared to %PRSDR value indicate good repeatability of the measurement (Irdawati et al., 2015). The calculation results on the $NaNO_3$ electrolyte yield a %RSDR of 7.08% and a %PRSDR of 4%. Consequently, the repeatability value is 1.77. Although the %RSDR value obtained in this measurement is higher than the %PRSDR value, the HorRat value remains below 2. Hence, the electrode demonstrates good stability in glucose analysis.

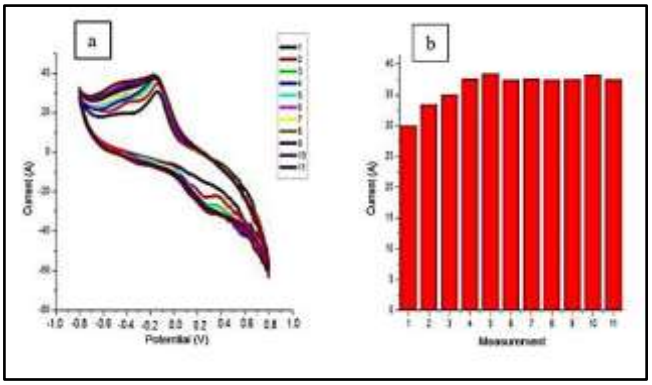

Figure 15. a) Voltammogram of measurement repeatability b) Histogram of measurement repeatability

Life time test on EPG/Mn_xO_y performance in glucose determination

Electrode age test is a test conducted to determine the stability of the electrode over a long period of time that is still suitable for use in analyzing an analyte. The electrode age test was carried out by measuring the graphene/Mn_xOy electrode on glucose for 15 days with a measurement period of once a day. The measurement results are shown in Figure 16.

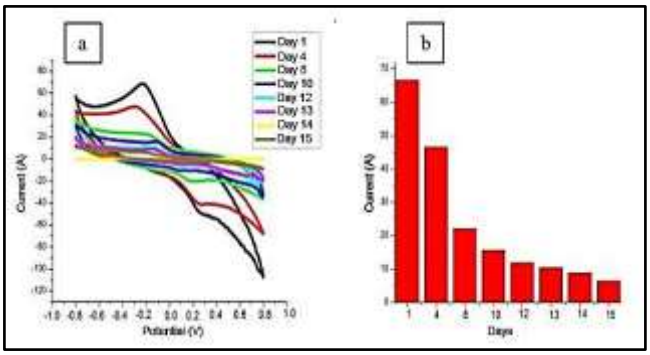

Figure 16. (a) Electrode life time voltammogram (b) Electrode age histogram

Based on the measurement results, the electrode demonstrated initial good condition on the first day, as indicated by the high peak current produced. On the 4th day, there was a slight decrease in the peak current, although not significantly. Subsequent tests conducted from the 8th to the 15th day showed a further decrease in peak current. This decrease can be attributed to the continuous use of the electrode, leading to the thickening of the diffusion layer on the electrode surface due to prolonged contact with

the test solution. According to Irdawati et al., (2015), this thickening results in a slower electron transfer, ultimately leading to a decrease in the peak current generated. Additionally, the decline in electrode response could also be attributed to the electrode's tendency to decay and become unstable at room temperature after prolonged storage (Khani et al., 2010).

CONCLUSION

The SEM characterization results reveal the presence of manganese oxide particles on the graphene sheet. The EDX results show a composition of 53.60% carbon, 15.45% oxygen, and 6.26% manganese. XRD analysis of the doped graphene exhibits peaks corresponding to Mn_3O4 (30.57, 44.39), MnO_2 (34.14), and MnO (39.85, 57.85, 68.94). The FTIR spectrum demonstrates a Mn-O interaction at a wave number of 615.29 cm^{-1}, and the loss of several functional groups after doping indicates the successful reduction of graphene by manganese ions. The optimal electrode composition is a composition of graphene:Mn (0.8:0.5), as evidenced by a peak anodic current (I_{pa}) of 122 µA. Other factors influencing the performance of the graphene/Mn_xO_y electrode include the supporting electrolyte and scan rate. The most favorable conditions for measuring glucose compounds using the graphene/Mn_xO_y electrode are a 0.1 M $NaNO_3$ electrolyte and a scan rate of 0.05 V/s. The detection limit achieved from EPG/Mn measurement for glucose is 4.45×10^{-5} M, with a repeatability value of 1.77. A repeatability value below 2 indicates a good repeatability of measurement in the analysis of glucose compounds.

REFERENCES

Adhytiawan, A. A., & Susanti, D. (2015). Pengaruh Variasi Waktu Tahan Hidrotermal Terhadap Sifat Kapasitif Superkapasitor Material Graphene. *Jurnal Teknik ITS*, *4*(1), F45–F50. https://doi.org/10.12962/j23373539.v4i1.8709

Agusu, L., & Yuliana. (2017). Fabrikasi komposit graphene/TiO2/PAni sebagai bahan elektroda baterai lithium-ion (Li-Ion). *Jurnal Aplikasi Fisika*, *13*(1). Retrieved from http://ojs.uho.ac.id/index.php/JAF/article/view/1862

Alanezi, K. M., Ahmad, I., AlFaify, S., Ali, I., Mohammad, A., Jabir, M. S., … Almutairi, F. M. (2024). A review of advanced heteroatom-doped graphene and its derivatives materials for photocatalytic applications. *Journal of Industrial and Engineering Chemistry*. https://doi.org/10.1016/j.jiec.2024.08.029

Alimin, A., Narsito, N., Kartini, I., & Santosa, S. J. (2015). Production of Silver Nanoparticle Chains inside Single Wall Carbon Nanotube with a Simple Liquid Phase Adsorption. *Bulletin of Chemical Reaction Engineering & Catalysis*, *10*(3), 266–274. https://doi.org/10.9767/bcrec.10.3.8416.266-274

Arifiyana, D., & Murwani, I. K. (2013). Pengaruh Doping Logam Fe pada CaF2 terhadap Struktur Ca1-xFexF2. *Jurnal Sains dan Seni ITS*, *2*(2), C54–C56. https://doi.org/10.12962/j23373520.v2i2.4305

Ayati, M. H., Araj-Khodaei, M., Haghgouei, T., Ahmadalipour, A., Mobed, A., & Sanaie, S. (2023). Biosensors: The nanomaterial-based method in detection of human gut microbiota. *Materials Chemistry and Physics*, *307*, 127854. https://doi.org/10.1016/j.matchemphys.2023.127854

Bantounou, M. A., Shoaib, K., Mazzoleni, A., Modalavalasa, H., Kumar, N., & Philip, S. (2024). The association between type 2 diabetes mellitus and Parkinson's disease; a systematic review and meta-analysis. *Brain Disorders*, *15*, 100158. https://doi.org/10.1016/j.dscb.2024.100158

Chung, D. Y., Heaney, P. J., Post, J. E., Stubbs, J. E., & Eng, P. J. (2023). Synchrotron X-ray diffraction of pyrolusite (MnO2) and rutile (TiO2) during heating to ~1000 °C. *Journal of Physics and Chemistry of Solids*, *177*, 111284. https://doi.org/10.1016/j.jpcs.2023.111284

Esfandiari, N., & Aliofkhazraei, M. (2024). Advances in the determination of trace amounts of iron cations through electrochemical methods: A comprehensive review of principles and their limits of detection. *Talanta*, *277*, 126365. https://doi.org/10.1016/j.talanta.2024.126365

Han, G. E., & Priefer, R. (2023). A systematic review of various pKa determination techniques. *International Journal of Pharmaceutics*, *635*, 122783. https://doi.org/10.1016/j.ijpharm.2023.122783

Hummers, W. S. Jr., & Offeman, R. E. (1958). Preparation of graphitic oxide. *Journal of the American Chemical Society*, *80*(6), 1339–1339. https://doi.org/10.1021/ja01539a017

Ilhami, M. R., & Susanti, D. (2014). Pengaruh Massa Zn Dan Temperatur Hydrotermal Terhadap Struktur Dan Sifat Elektrik Material Graphene. *Jurnal Teknik ITS*, *3*(2), F185–F190. https://doi.org/10.12962/j23373539.v3i2.6610

Irdawati, I., Manurung, M., & Septiawan, K. A. (2015a). Deteksi dopamin secara voltametri menggunakan elektroda pasta karbon termodifikasi eter mahkota (dibenzo-18-crown-6). *Jurnal Kimia Mulawarman*, *12*(2), 68–74. https://doi.org/10.30872/jkm

Kamal, M. A., & Klein, P. (2011). Determination of sugars in honey by liquid chromatography. *Saudi Journal of Biological Sciences*, *18*(1), 17–21. https://doi.org/10.1016/j.sjbs.2010.09.003

Li, M., Kuang, S., Kang, Y., Ma, H., Dong, J., & Guo, Z. (2022). Recent advances in application of iron-manganese oxide nanomaterials for removal of heavy metals in the aquatic environment. *Science of The Total Environment*, *819*, 153157. https://doi.org/10.1016/j.scitotenv.2022.153157

Liang, X., Jiang, M., Zhan, F., Zu, Y., Wang, X., & Feng, X. (2024). Influence of preparative parameters on the morphology and reactivity of synthetic hexagonal birnessite. *Applied Geochemistry*, *172*, 106116. https://doi.org/10.1016/j.apgeochem.2024.106116

Mira, P. V., Mahmudin, L., & Iqbal, I. (2018). Sintesis dan Analisis Sifat Magnetik Nanopartikel Magnetit (Fe3o4) Berbasis Pasir Besi. *Gravitasi*, *17*(2). https://doi.org/10.22487/gravitasi.v17i2.12420

Nur Ashakirin Binti Mohd Nashruddin, S., Hani Mohamed Salleh, F., & Ayunni Mohd Raub, A. (2024). Early detection of kidney problems through voltammetry, potentiometry, amperometry, and impedance electrochemical techniques: A comprehensive review. *Measurement*, *230*, 114475. https://doi.org/10.1016/j.measurement.2024.114475

Othman, F. E. C., Nordin, N. A. H. Md., Ismail, N., Zakria, H. S., Junoh, H., & Aziz, Mohd. H. Abd. (2024). A review on sustainable graphene production from rice husks: Strategies and key considerations. *Chemical Engineering Journal*, *497*, 154408. https://doi.org/10.1016/j.cej.2024.154408

Ratnayani, K., Adhi, D., & Gitadewi, I. (2008). Penentuan kadar glukosa dan fruktosa pada madu randu dan madu kelengkeng dengan metode kromatografi cair kinerja tinggi. *Jurnal Kimia*, *2*(2), 77–86.

R. Dreyer, D., Park, S., W. Bielawski, C., & S. Ruoff, R. (2010). The chemistry of graphene oxide. *Chemical Society Reviews*, *39*(1), 228–240. https://doi.org/10.1039/B917103G

Shao, G., Lu, Y., Wu, F., Yang, C., Zeng, F., & Wu, Q. (2012). Graphene oxide: The mechanisms of oxidation and exfoliation. *Journal of Materials Science*, *47*(10), 4400–4409. https://doi.org/10.1007/s10853-012-6294-5

Sharma, R., Jaiswal, S., Chauhan, R., Bhardwaj, M., Verma, K., Dwivedi, J., & Sharma, S. (2024). Applications of graphene-based photocatalysts for efficient functionalized degradation of some common antibiotics. *Inorganic Chemistry Communications*, *168*, 112941. https://doi.org/10.1016/j.inoche.2024.112941

Song, N.-J., & Ma, C. (2018). A Green Synthesis of Mn3O4/graphene Nanocomposite as Anode Material for Lithium-Ion Batteries. *International Journal of Electrochemical Science*, *13*(1), 452–460. https://doi.org/10.20964/2018.01.01

Stoller, M. D., Park, S., Zhu, Y., An, J., & Ruoff, R. S. (2008). Graphene-Based Ultracapacitors. *Nano Letters*, *8*(10), 3498–3502. https://doi.org/10.1021/nl802558y

Taufantri, Y., Irdhawati, I., & Asih, I. A. R. A. (2016). Sintesis dan Karakterisasi Grafena dengan Metode Reduksi Grafit Oksida Menggunakan Pereduksi Zn. *Jurnal Kimia Valensi*, *2*(1), 17–23.

Wang, J., Zheng, Y., Huang, H., Ma, Y., & Zhao, X. (2024). An overview of signal amplification strategies and construction methods on phage-based biosensors. *Food Research International*, *191*, 114727. https://doi.org/10.1016/j.foodres.2024.114727

Wong, R. A., Yokota, Y., & Kim, Y. (2022). Stepping beyond cyclic voltammetry: Obtaining the electronic and structural properties of electrified solid–liquid interfaces. *Current Opinion in*

Electrochemistry, *34*, 100964. https://doi.org/10.1016/j.coelec.2022.100964

Zhang, W., & Cheng, C. Y. (2007). Manganese metallurgy review. Part I: Leaching of ores/ secondary materials and recovery of electrolytic/chemical manganese dioxide. *Hydrometallurgy*, *89*(3), 137–159. https://doi.org/10.1016/j.hydromet.2007.08.010